Optimal Eco-Routing for Hybrid Vehicles with Mechanistic/Data-Driven Powertrain Model Embedded

Adrian Caspari[a], Steffen Fahr[a], Alexander Mitsos*[,b,a,c]

[a]Process Systems Engineering (AVT.SVT), RWTH Aachen University, 52074 Aachen, Germany
[b]JARA-ENERGY, 52056 Aachen, Germany
[c]Energy Systems Engineering (IEK-10), Forschungszentrum Jülich, 52425 Jülich, Germany

date: June 12, 2021

Abstract: Hybrid Electric Vehicles (HEVs) are regarded as an important (transition) element of sustainable transportation. Exploiting the full potential of HEVs requires (i) a suitable route selection and (ii) suitable power management, i.e., deciding on the split between combustion engine and electric motor usage as well as the mode of the electric motor, i.e., driving or charging the battery (recuperation). The coupling of the two subproblems motivates to formulate the routing and power management as an integrated optimization problem, i.e., optimizing simultaneously the route selection and the split between combustion engine and electric motor over the entire route selection.
We present an eco-routing approach that embeds a hybrid (mechanistic/data-driven) model of the HEV powertrain in an integrated routing and power management optimization problem. The hybrid model uses mechanistic equations for those parts of the powertrain that can easily be modeled with mechanistic equations and data-driven surrogates for those parts of the powertrain that are difficult to model mechanistically and to solve. Formulating the integrated routing problem with the hybrid model yields a mixed-integer bilinear program which we reformulate and solve a mixed-integer linear program using a state-of-the-art solver.
The results show the validity of the developed hybrid powertrain model and demonstrate that the eco-routing approach with powertrain model embedded can be applied on large-scale problems. We consider optimization for minimal travel time and minimum fuel consumption. The latter results in fuel demand reductions up to 70 %. Alternatively we minimize the fuel consumption while constraining the travel time to a maximum value resulting in up to 50 % fuel demand reductions. The highest fuel demand reductions are achieved in urban environments. The entire framework is written in python and provided as an open-source version (MIT License) under https://git.rwth-aachen.de/avt-svt/public/optimal-routing that can readily be applied.

Keywords: optimal vehicle routing and operation, hybrid vehicles, fuel demand reduction, eco routing, MILP, mechanistic/data-driven modeling, carbon footprint reduction

1 Introduction

Hybrid electric vehicles (HEVs) have been regarded as the avenue towards the ultimate ecologically friendly car for more than a decade [1]. They offer several advantages when compared to fully electric vehicles (EVs): HEVs are cheaper, they offer more robust distance ranges, and they do not necessarily require a charging infrastructure. As EVs, they can be used for electricity grid services enabled by the electricity buffer that they provide [2]. Compared to conventional vehicles relying on internal combustion engines only, they can be used to shift emissions towards preferred locations, thereby helping to reduce the emissions in heavy traffic regions. Moreover, including a hybrid vehicle powertrain allows for downsizing the combustion engine without sacrificing peak power. By employing a suitable power split, a smaller engine can run closer to its optimal operation point, thereby ultimately increasing the powertrain efficiency. Nevertheless, HEVs are associated currently with the highest lifetime carbon footprint among the common vehicle technologies, i.e., electric, compressed natural gas, fuel cells, diesel, and even gasoline based vehicles [3]. The high carbon footprint of HEVs might impede the further market penetration. Re-

*A. Mitsos, AVT Process Systems Engineering, RWTH Aachen University, 52074 Aachen, Germany, E-mail: amitsos@alum.mit.edu

ducing the high carbon footprint of HEVs is, hence, required to actually make them ecologically friendly and to further gain acceptance of the HEV technologies.

A carbon footprint reduction can be achieved by eco routing strategies, i.e., selecting the route leading to the minimum fuel demand. The fuel demand depends on the HEV power management, which is deciding on split between engine and electric motor usage as well as the mode of the electric motor (discharging or charging of the battery). Consequently, eco routing strategies have to consider the power management. At the same time, optimal power management should take into account the remaining route. This motivates to formulate the routing and power management as an integrated optimization problem. As the power management has to decide on the usage of the battery, the integrated problem has to satisfy battery capacity constraints expressed by the state of charge (SOC) of the battery. Thus, fuel demand and SOC have to be modeled to predict their behavior for a route and power management.

While numerous works have been published on HEV power management and velocity control over fixed routes, e.g., [4–6], there are few works which considered the integrated optimization problem of eco routing and power management [7–16].

Guanetti et al. [7] formulated an eco routing problem for plug-in HEVs as a resource constrained shortest path problem based on simple linear correlations for the engine and battery power demand. They formulated two routing problem, a static and a dynamic routing problem, depending on whether the routing problem uses static or dynamic traffic speed forecasts. They considered a powertrain with two operation modes, charge depleting mode and charge sustaining mode, i.e., the combustion engine cannot be used to charge the battery. Furthermore, vehicle powertrain used a fixed order of operation modes, i.e., the operation modes cannot be selected by the solution of the routing optimization problem.

Nejad et al. [8] proposed routing algorithms for plug-in HEVs, which considers operation mode selection during route planning based on simple linear correlations for fuel demand and battery discharge. They formulate the integrated optimal routing and operation mode selection problem as a shortest path problem and provide full polynomial time approximations for the problem. The resource selection is mutually exclusive, i.e., their approach can select either electric motor or combustion engine as energy source but not both resources together. However, there can be cases where fuel savings can be realized by using both engine and motor at the same time.

Strehler et al. [9] presented a routing approach for electric vehicles and HEVs considering intermediate stops at charging stations, formulated as a resource constrained shortest path problem. Their approach considers Pareto-optimal strategies, which requires an expression for the Pareto front with regard to battery charge and fuel demand on every road segment parameterized depending on the choice of the operation mode.

Houshmand and Cassandras [10] and Houshmand et al. [11] presented an integrated optimal routing and powertrain management approach for plug-in HEVs. They used simple linear correlations for the battery charge and fuel demand, i.e., they do not embed a powertrain model in the routing optimization problems. Considering two operation modes, a charge sustaining mode and a charge depletion mode, i.e., charging the battery with the energy from the combustion engine is not covered. Their integrated optimal routing and powertrain management approach selects the route and switches between the charge depletion mode and the charge sustaining mode. The approach can not account for accurate dynamic SOC behavior.

Zhen et al. [12] presented an HEV routing approaching to plan the routes for several HEVs based on simple linear correlations for battery charge and fuel demand. The approach selects between four HEV modes, however, neglects battery charging due to recuperation.

Kurtulus and Inhalan [13] presented a routing approach for HEVs considering battery wear. A mechanistic power train model is used to calculate in a serial manner the cost in form of a weighted sum of distance, time, energy demand, and battery wear on every arc. I.e., the powertrain model is not embedded in the routing optimization problem. As a consequence, the approach does not integrate optimal routing and vehicle operation.

Salazar et al. [14] presented an approach for integrated optimal route planning and operation for plug-in HEVs. Using a hybrid (mechanistic/data-driven) model, they calculated Pareto frontiers in the relative fuel and batter charge demand on every arc a priori. In the actual routing optimization problem, they embed a piecewise linear approximation of the Pareto frontiers. I.e., they do not embed the hybrid model in the routing optimization problem but a surrogate representation of the Pareto frontiers. Although

leading to fast computational times for the solution of the resulting optimization problems, the approach, hence, cannot account for detailed SOC behavior, where the change in the SOC depends on the SOC itself.
De Nunzio et al. [15] presented an approach for integrated optimal route planning and powertrain management based on a semi-analytical solution of the powertrain model. The semi-analytical solution consists of a surrogate for the battery SOC and a semi-analytical model for the fuel demand using predefined velocity profiles. I.e., no powertrain model is embedded in the routing optimization problem and the approach cannot account for detailed SOC behavior, where the change in the SOC depends on the SOC itself.
De Nunzio et al. [16] presented a general constrained optimization framework for optimal routing of HEVs and compared different solution strategies to solve the respective optimization problem. In the routing problem, they assumed suitable powertrain energy management, i.e., they do not embed a powertrain model in the routing problem.

The cited prior art works [7–16] did not embed a (physics based) model of the powertrain in the eco routing optimization problems. In particular, they did not embed dynamic equations, e.g., for the battery SOC. Rather, they used correlations to predict the HEV fuel demand and SOC. They used simplified linear correlations to predict the SOC behavior or a battery energy content model instead, although the SOC has characteristics which can be described mechanistically by (linear) differential equations, that can easily be embedded in an optimization problem, as we show in this work. While [13] did not explicitly account for the powertrain in the routing and, hence, did not consider the HEV operating modes in the routing directly, [7–12,15,16] considered predefined operation modes or operating strategies, and only [14] considered the operation modes entirely as a degree of freedom in the routing optimization problem.

In contrast to the existing works, we target an eco routing strategy which embeds a hybrid powertrain model in the routing optimization problem, in order to explore the prediction and extrapolation capability associated with a physical based powertrain model. We formulate a general routing problem as a dynamic optimization problem. To make the eco routing problem computationally tractable, we develop, validate, and embed a hybrid model, cf., e.g., [17,18], of the powertrain based on a mechanistic powertrain model. The model uses a differential equation to predict the SOC, which is derived from a mechanistic SOC model. The routing takes place on a route map formulated as a directed graph including topology information comprising speed limits and local elevations. Using the powertrain model embedded in the eco routing optimization problem allows us to consider the operating modes of the HEV as a degree of freedom, i.e., there is no restriction to predefined operating modes only. Rather, we can exploit the full operational range of the hybrid powertrain. The resulting integrated eco routing and powertrain management optimization problem with the hybrid powertrain model is a mixed-integer bilinear program (MIBP) which, after making some assumptions (in particular, quasi-stationarity for the HEV velocity), we reformulate to and solve as a mixed-integer linear program (MILP).

The remainder of the work is structure as follows. Section 2 summarizes the directed graph formulation. Section 3 presents the model of the vehicle powertrain and the development of a hybrid powertrain model. Section 4 presents the formulation for the integrated optimal routing and powertrain management optimization problem. We apply the integrated optimal routing and powertrain management approach to three case studies an explain the results in Section 5. Finally, we draw conclusions in Section 6.

2 Directed Graph

We formulate the road network as a directed graph $\mathcal{G} = (\mathcal{N}, \mathcal{A})$ comprising of the set of nodes $\mathcal{N} = \{1, ..., N_\mathrm{N}\}$ and set of arcs $\mathcal{A}$ with the cardinality $|\mathcal{A}| = N_\mathrm{A}$, which correspond to the set of road intersections and set of road segments, respectively. The directed graph representation of road maps is standard in routing and has also been used, e.g., by [10]. The nodes are associated with their latitude, longitude, and elevation. The set of arcs $\mathcal{A}$ comprises of the arcs (i, j) which are the connections from node i to node j with $i, j \in \mathcal{N}$. An arc $a = (i, j)$ is associated with the road type, arc length l_a, average slope angle α_a, and speed limit $\bar{v}_a$. The arc length, arc speed limits, latitude and longitude of nodes, and elevation of nodes can be obtained, e.g., from OpenStreetMap [19] or open-elevation [20]. The average slope angle α_a of an arc $a = (i, j)$ can be calculated using the length of an arc $a = (i, j)$, and altitudes of the nodes

i and j, wherein we assume that an arc $a = (i, j)$ connects the nodes i and j as a straight line with a constant slope. We store the information about the correlation between nodes and edges in a directed graph in the following matrices:

$$E_{n,a} = \begin{cases} 1 & \text{if arc } a \text{ enters node } n, \\ 0 & \text{otherwise,} \end{cases}$$

$$L_{n,a} = \begin{cases} 1 & \text{if arc } a \text{ leaves node } n, \\ 0 & \text{otherwise,} \end{cases}$$

$$S_n = \begin{cases} 1 & \text{if } n \text{ is end node,} \\ -1 & \text{if } n \text{ is start node,} \\ 0 & \text{otherwise.} \end{cases}$$

For the routing optimization problem, we introduce a binary variable $\boldsymbol{x} \in \{0,1\}^{N_A}$, indicating the route selection: $x_a = 1$ in case the selected route includes the arc a, and $x_a = 0$ otherwise. Using this variable, we can formulate the following constraints to select a valid route:

$$\sum_{a \in \mathcal{A}} (E_{n,a} - L_{n,a}) \cdot x_a = S_n, \ \forall \ n \in N,$$

which guarantees that the route starts in the start node, ends in the end note, and that the other nodes are entered as many times as they are left, and

$$\sum_{a \in \mathcal{A}} (E_{n,a} + L_{n,a}) \cdot x_a \leqslant 2, \forall n \in \mathcal{N},$$

to avoid the route includes cycles, i.e., a node n can be entered and left only once. We assume that in most practical applications, cycles are suboptimal in eco routing, and we can imagine only few pathological examples, where cycles would be advantageous, which we avoid by using these constraints. Adding these constraints makes the optimization problem easier to solve, as cycles, which are suboptimal solutions in most practical applications, are excluded.

3 Vehicle Model

In this section, we describe the hybrid vehicle powertrain model, which we use to predict the vehicle behavior on every arc a during the routing optimization. The hybrid model is based on a mechanistic powertrain model. The equations for the mechanistic powertrain model are taken from [21] and we refer the reader to this work for a detailed overview and derivation of the equations. Fig. 1 shows a schematic of the powertrain model. While we focus on this particular powertrain architectures, the approach can be applied to other architectures, in particular, when the gear box is coupled in series with the engine, i.e., the electric power train part is not directly affected by the gear selection. Further, the approach uses engine and battery characteristics which can easily be exchanged in case of other vehicles with the same architecture. We formulate the model to allow for subsequent equation-oriented optimization. The first part of the model comprises equations for the required transition force, which follows from the map topology and dynamics of motion of the vehicle, independently of how the required transition force is provided by the vehicle. The required transition force has to be provided by the powertrain of the vehicle. Here, we consider a parallel hybrid electric powertrain shown in Fig. 1. The same powertrain architecture has been used in previous works, e.g., [14]. The powertrain comprises an electric and a combustion powertrain. Both of them are connected to the street via a torque split, a differential, and the wheels, which finally transmit the required transition force generated by the power train to the street. Our hybrid model has the same structure as the powertrain architecture. In the routing optimization problem, the vehicle model has to be solved on every arc $a = (i, j) \in \mathcal{A}$ of the graph $\mathcal{G} = (\mathcal{N}, \mathcal{A})$, described in Section 2. We omit the index in the model formulation indicating the arc a on which the model is

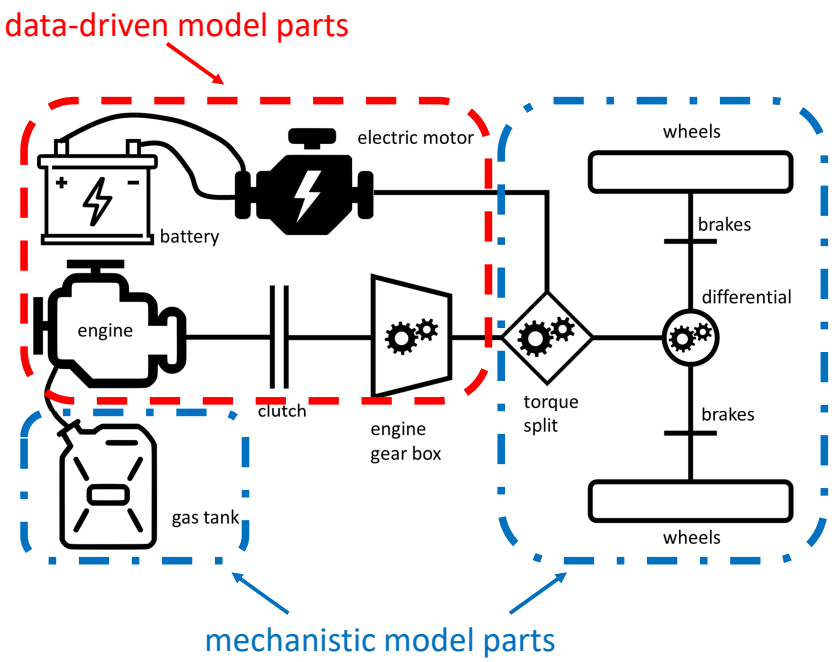

Fig. 1: Parallel-hybrid powertrain configuration. Adapted from [14].

solved for conciseness but point out that every model variable/state is indexed over the arcs in the later routing optimization problem.

In Section 3.1, we describe the required transition force first, before we show the equations connecting the force with the electric and combustion powertrain via the differential and the torque split. Afterwards, we describe the electric powertrain in Section 3.2 and the combustion powertrain in Section 3.3.

3.1 Required Transition Force

We calculate the required transition force that has to be provided by the vehicle in order to drive based on the acceleration of the vehicle and the force acting on it. Fig. 2 illustrated the forces acting on the vehicle moving with the velocity v including the aerodynamic friction F_{a}, rolling friction F_{r}, force caused by the gravity F_{g}, and the required traction force F_{req}. The aerodynamic resistance force is calculated by

$$F_{\mathrm{a}}(t) = \frac{1}{2}\rho_a A_f c_d v(t)^2, \tag{1}$$

with the ambient air density ρ_a, the frontal area of the vehicle A_f, the drag coefficient c_d, and the vehicle speed v. Note that the drag coefficient c_d is assumed to be constant for convenience. Alternatively, it can depend on the velocity. In case that the velocity is assumed constant over an arc, as we do later, the drag coefficient on an arc can be precalculated based on the respective velocity on the arc. The rolling friction force is calculated by

$$F_{\mathrm{r}}(t) = c_r m_v g \cos(\alpha(t)), v > 0,$$

with the rolling friction coefficient c_r, the vehicle mass m_v, the gravity acceleration g, and the road angle to the horizontal α. The gravity force projection in the direction of motion is calculated by

$$F_{\mathrm{g}}(t) = m_v g \sin(\alpha(t)).$$

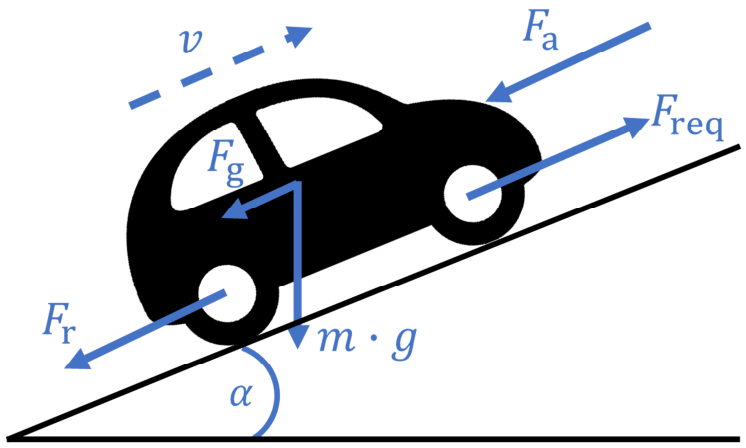

Fig. 2: Forces acting on vehicle of during transition in direction of v (dashed arrow).

Using these forces, the longitudinal dynamics of the vehicles are described by the equation

$$m_v \left.\frac{\mathrm{d}v}{\mathrm{d}t}\right|_t = F_{\mathrm{req}}(t) - (F_{\mathrm{a}}(t) + F_{\mathrm{r}}(t) + F_{\mathrm{g}}(t)). \tag{2}$$

We can calculate the travel distance s using

$$\left.\frac{\mathrm{d}s}{\mathrm{d}t}\right|_t = v(t). \tag{3}$$

The velocity v results from the vehicle acceleration a

$$\left.\frac{\mathrm{d}v}{\mathrm{d}t}\right|_t = a(t).$$

The required transition force F_{req} is transferred via the wheels and differential to the torque splitter according to

$$T_{\mathrm{tc}}(t)\gamma = r_w F_{\mathrm{req}}(t) + T_{\mathrm{brake}}(t), \tag{4}$$

with the wheel radius r_w, the wheel torque T_w, the gear ration γ, the brake torque $T_{\mathrm{brake}} \geqslant 0$, and the torque entering the torque coupler T_{tc}. In (4) we assume perfect transformation, i.e., without any loss, as is commonly done, cf., e.g., [21]. The wheel torque T_w and the required traction force F_{req} may be positive or negative. In particular, F_{req} may be negative if the vehicle drives downhill and T_{tc} may be negative if the battery is recharged by the electric motor due to recuperation. We calculate the rotational speed ω_{tc} of the torque coupler as

$$\omega_{\mathrm{tc}}(t) \cdot r_w = v(t) \cdot \gamma.$$

The torque coupler couples the incoming torque T_{tc}, the incoming torque of the gear box T_{gb}, and the torque of the electric motor T_{m} according to

$$T_{\mathrm{gb}}(t) + T_{\mathrm{m}}(t) = T_{\mathrm{tc}}(t),$$

and the rotational speed of the torque coupler ω_{tc}, the rotational speed to the engine gear box ω_{gb}, and the rotational speed of the electric motor ω_{m} according to

$$\begin{aligned} \omega_{\mathrm{tc}}(t) &= \omega_{\mathrm{m}}(t), \\ \omega_{\mathrm{tc}}(t) &= \omega_{\mathrm{gb}}(t). \end{aligned}$$

3.2 Electric Powertrain

We model the electric powertrain using data-driven/empirical models for the electric motor and for the battery.

3.2.1 Electric Motor

We model the electric motor (generator during recuperation) using the Willans approach [21, 22]:

$$T_m(t) \cdot \omega_m(t) = \begin{cases} P_m(t) \cdot \eta_m - P_{m,0}, \text{if } P_m(t) > 0, \\ P_m(t)/\eta_m - P_{m,0}, \text{if } P_m(t) \leqslant 0, \end{cases} \tag{5}$$

with the electric motor efficiency η_m and the base load $P_{m,0}$ as parameters. For an electric motor, constant values for these parameters are justified in a broad operation range [22]. In the routing optimization problem, we formulate the Willans approach for the electric motor (5) using the binary formulation

$$T_\mathrm{m}(t) \cdot \omega_\mathrm{m}(t) = \beta(t) \cdot (P_\mathrm{m}(t) \cdot \eta_\mathrm{m} - P_{\mathrm{m},0}) + (1 - \beta(t)) \cdot (P_\mathrm{m}/\eta_\mathrm{m} - P_{\mathrm{m},0}), \tag{6a}$$

$$(1 - \beta(t)) \cdot P_\mathrm{m}(t) \leqslant 0, \tag{6b}$$

$$-\beta(t) \cdot P_\mathrm{m}(t) \leqslant 0, \tag{6c}$$

with the auxiliary binary variable $\beta(t) \in \{0, 1\}$, which equals one, if the power demand of the motor $P_\mathrm{m} > 0$ (motor contributes to vehicle transition), and zero otherwise (motor used to charge the battery due to recuperation). Alternatively, the nonsmooth electric motor model (5) could be formulated using complementarity constraints or nonlinear complementarity problem functions, cf., e.g., [23].

3.2.2 Battery Model

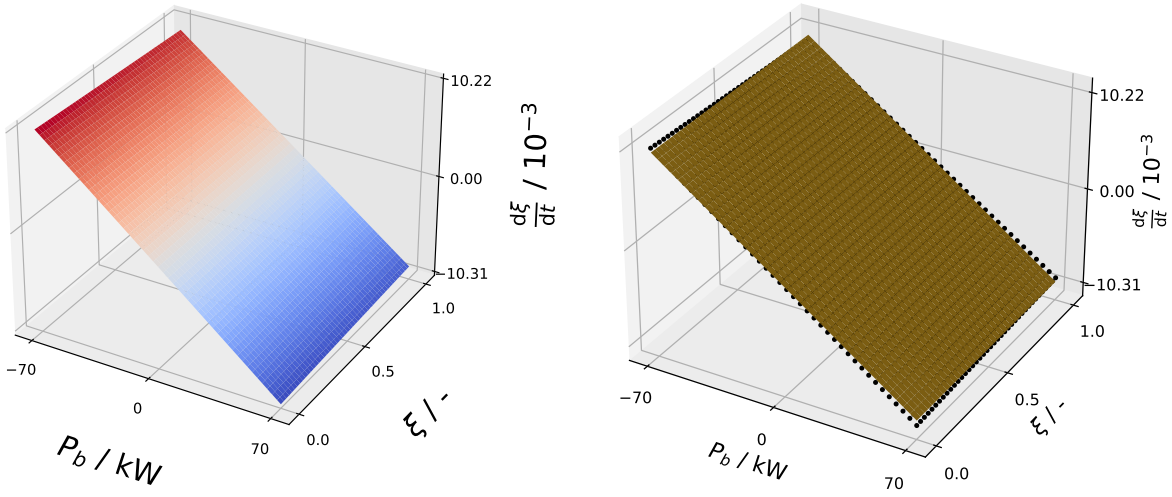

(a) (b)

Fig. 3: Battery characteristic for $\kappa_1 = 250$ V, $\kappa_2 = 20.0$ V, $\kappa_3 = 0.20\ \Omega$, $\kappa_4 = $-0.05 Ω, $Q_0 = 45{\cdot}3600$ As, $\eta_C = 0.95$. (a) Battery characteristic as solution of (7). (b) Quadratic function fit of characteristic. Black points samples from battery characteristic as solution of (7). Surface plot from quadratic polynomial regression of (8).

The power demand of the electric motor is provided by the battery:

$$P_\mathrm{m}(t) = P_\mathrm{b}(t),$$

with the battery terminal power P_b.

Batteries can be modeled as an equivalent electric circuit [21] using the following equations:

$$U_\mathrm{b}(t) \cdot I_\mathrm{b}(t) = P_\mathrm{b}(t), \tag{7a}$$
$$Q_0 \cdot \xi_\mathrm{b}(t) = Q_\mathrm{b}(t), \tag{7b}$$
$$\left.\frac{d\xi}{dt}\right|_t = -\frac{\eta_c \cdot I_\mathrm{b}(t)}{Q_0}, \tag{7c}$$
$$U_\mathrm{b}(t) = \frac{U_\mathrm{b0}(t)}{2} + \sqrt{\frac{U_\mathrm{b0}^2(t)}{4} - P_\mathrm{b}(t) \cdot R_\mathrm{b}(t)}, \tag{7d}$$
$$U_\mathrm{b0}(t) = \kappa_2 \cdot \xi_\mathrm{b}(t) + \kappa_1, \tag{7e}$$
$$R_\mathrm{b}(t) = \kappa_4 \cdot \xi_\mathrm{b}(t) + \kappa_3, \tag{7f}$$

with the Coulombic efficiency η_c, the electric charge Q_b, the SOC ξ_b, the discharge current I_b, the voltage $U_\mathrm{b} \geqslant 0$, the maximum battery capacity Q_0, and the parameters κ_1, κ_2, κ_3, κ_4. Note that (7b) is the defining equation for the SOC ξ_b. The model neglects the wearing effects or the effect of the battery temperature on its behavior.

The battery model (7) is a nonlinear DAE that would complicate the routing optimization problem if embedded. Therefore, we derive a linear differential equation for the battery using polynomial regression. The resulting linear differential equation can easily be embedded in an optimization problem, e.g., using collocation [24] or using the analytical solution of the linear differential equation. To derive the linear differential equation, we generate the data first. Therefore, we solve (7) using Dymola [25] (using the battery model parameters presented in Table 1) leading to the data plotted in Fig. 3a. Afterwards, we perform polynomial regression on this data with Matlab's polynomial curve fitting [26] to describe the function $f(P_\mathrm{b}(t), \xi(t))$ as a linear function and obtain a linear differential equation of the following form:

$$\left.\frac{\mathrm{d}\xi}{\mathrm{d}t}\right|_t = p_{\mathrm{b},0} + p_{\mathrm{b},1} \cdot \xi(t) + p_{\mathrm{b},2} \cdot P_\mathrm{b}(t), \tag{8}$$

with the parameter values obtain from polynomial regression $\boldsymbol{p}_\mathrm{b} = (-4.1014 \cdot 10^{-6},\ 2.0193 \cdot 10^{-6},\ -139.6228 \cdot 10^{-6}/\mathrm{kW})$. The fit is shown in Fig. 3b. We see that the expression (8) can approximate the battery characteristics described by (7) very well.

Note that we could use higher order polynomials instead. However, using the linear function is advantageous, in particular, as the routing optimization problem the vehicle model embedded is a MILP instead of mixed-integer nonlinear program due to the presence of higher order polynomials. In particular, under the assumption that the velocity v is time-invariant, the power demand of the battery P_b is time-invariant as well, and the analytical solution of (8) is a linear algebraic equation, which can easily be embedded in an optimization problem.

3.3 Combustion Powertrain

The combustion powertrain model consists of the mechanistic model for the fuel demand and a data-driven model for the engine and the gear box. The data-driven model for the engine and gear box is based on an optimization problem minimizing the engine power demand by selecting the gear of the gear box. Embedding this model corresponds, hence, to an optimal gear selection for minimum engine power demand.

3.3.1 Fuel Demand Model

We calculate the fuel demand m_fuel using the following differential equation

$$\left.\frac{\mathrm{d}m_\mathrm{fuel}}{\mathrm{d}t}\right|_t = P_\mathrm{e}(t)/H_\mathrm{fuel},$$

with the energy content of the fuel H_fuel.

3.3.2 Data-Driven Engine and Gear Box Model

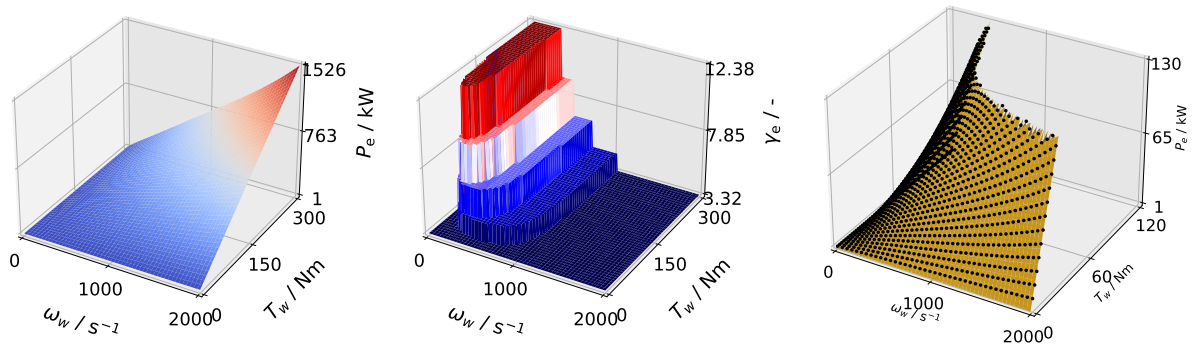

(a) (b) (c)

Fig. 4: Optimal engine power demand as function of rotational speed and torque before the engine gear. (a) Optimal engine power demand map. (b) Optimal gear ratio map. (c) Optimal engine power demand samples (black dots) and regressed polynomial for hybrid model, i.e., combined gear box and engine model (yellow surface).

Similar to electric motors, combustion engines can be modeled using the Willans approach [21, 22]:

$$T_\mathrm{e}(t) \cdot \omega_\mathrm{e}(t) = P_\mathrm{e}(t) \cdot \eta_\mathrm{e}(t) - P_{\mathrm{e},0}(t), \tag{9}$$

with the engine torque $T_\mathrm{e} \geqslant 0$, the engine rotational speed $\omega_\mathrm{e} \geqslant 0$, the engine power demand P_e, the engine efficiency η_e, and the engine base load $P_{\mathrm{e},0}$. In contrast to the Willans approach for the electric motor (5), the engine efficiency $\eta_\mathrm{e}(t)$ and the base load $P_{\mathrm{e},0}(t)$ depend on the rotational speed of the engine ω_e [22]. We use the following correlations in accordance with [22]:

$$\begin{aligned} P_{\mathrm{e},0}(t) &= \kappa_{\mathrm{e},1} \cdot \omega_\mathrm{e}(t) + \kappa_{\mathrm{e},0}, \\ \eta_\mathrm{e}(t) &= \kappa_{\mathrm{e},3} \cdot (\omega_\mathrm{e}(t) - \omega_\mathrm{e}^*)^2 + \kappa_{\mathrm{e},2}, \end{aligned} \tag{10}$$

with the parameters $\kappa_{\mathrm{e},0} \geqslant 0$, $\kappa_{\mathrm{e},1} \geqslant 0$, $\kappa_{\mathrm{e},2} \geqslant 0$, $\kappa_{\mathrm{e},3} \leqslant 0$, and $\omega_\mathrm{e}^* \geqslant 0$. The parameter ω_e^* indicates the rotational speed leading to the maximum engine efficiency η_e.

The gear box couples torque coupler and engine according to the equations

$$\begin{aligned} T_\mathrm{e}(t) \cdot \gamma_\mathrm{gb}(t) &= T_\mathrm{gb}(t), \\ \omega_\mathrm{gb}(t) \cdot \gamma_\mathrm{gb}(t) &= \omega_\mathrm{e}(t), \end{aligned} \tag{11}$$

with the engine gear ratio $\boldsymbol{\gamma}_\mathrm{gb}(t)$, which can be chosen from the set of gear ratios $\boldsymbol{\Gamma}_\mathrm{gb}$.

The engine and gear box models (9), (10), and (11) form a algebraic nonlinear equation system. In order to make the routing optimization problem computationally more tractable, we derive a bilinear polynomial to approximate the engine and gear box models as described in the following.

Given an engine torque entering the engine gear, rotational speed before the engine gear box, and engine gear, we can calculate the engine power demand P_e. We can, hence, minimize the engine power demand for a given rotational speed and torque entering the gear box by manipulating the gear of the engine gear box. This corresponds to an automatic gear selection minimizing the power demand of the combustion engine. Since the fuel demand directly correlates with the power demand of the engine, it is justified to embed an engine and gear box model with automatic gear selection for minimum power demand. Thus, we solve an optimization problems to minimize the engine power demand for given engine torque and rotational speed before the engine gear box (by manipulating the engine gear). The optimization problem is subject to the equations (9), (10), and (11). For a given gear box torque T_gb and

rotational speed ω_{gb}, the optimization problem are given by

$$\begin{aligned}
&\min_{\gamma_{\text{gb}}} P_{\text{e}},\\
&s.t. T_{\text{e}} \cdot \gamma_{\text{gb}} = T_{\text{gb}},\\
&\quad \omega_{\text{gb}} \cdot \gamma_{\text{gb}} = \omega_{\text{e}},\\
&\quad T_{\text{e}} \cdot \omega_{\text{e}} = P_{\text{e}} \cdot \eta_{\text{e}} - P_{\text{e},0},\\
&\quad P_{\text{e},0} = \kappa_{\text{e},1} \cdot \omega_{\text{e}} + \kappa_{\text{e},0},\\
&\quad \eta_{\text{e}} = \kappa_{\text{e},3} \cdot (\omega_{\text{e}} - \omega_{\text{e}}^{*})^2 + \kappa_{\text{e},2},\\
&\quad \gamma_{\text{gb}} \in \mathbf{\Gamma}_{\text{gb}},\\
&\quad P_{\text{e}} \in \mathbb{R}, T_{\text{e}} \in \mathbb{R}, \omega_{\text{e}} \in \mathbb{R}, \eta_{\text{e}} \in \mathbb{R}, P_{\text{e},0} \in \mathbb{R}.
\end{aligned} \tag{12}$$

The optimization problem (12) is a mixed-integer quadratically-constrained program (MIQCP), which we solve offline, not during the routing optimization problem solution. The problem can be solved offline since the gear selection only affects the fuel demand and can hence be used to minimize the fuel demand independently of the other parts of the vehicle powertrain. Solving this optimization problem using Gurobi [27] with Pyomo [28, 29], we obtain a map of the optimal engine power demand dependent on the torque and rotational speed before the engine gear box. The optimal engine power demand map is plotted in Fig. 4a and the optimal engine gear map is shown in Fig. 4b. Using Matlab's polynomial regression [26], we approximate the map shown in Fig. 4a by the following polynomial

$$P_{\text{e}}(t) = p_{\text{e},0} + p_{\text{e},1} \cdot \omega_{\text{gb}}(t) + p_{\text{e},2} \cdot T_{\text{gb}}(t) + p_{\text{e},3} \cdot T_{\text{gb}}(t) \cdot \omega_{\text{gb}}(t), \tag{13}$$

and obtain by the following parameter values after regression $\boldsymbol{p}_{\text{e}} = (1.2862{\cdot}10^3\ \text{W}, 4.5876\ \text{Nm}, 27.4552\ \text{s}^{-1}, 2.3882)$. The polynomial is regressed only for those samples for which $P_{\text{e}} \leqslant P_{\text{e}}^{\max}$ as this is the maximum engine power demand, which we use as a constraint in the route optimization problem. The regressed polynomial and used samples are shown in Fig. 4c. We see that the polynomial of the form (13) approximates the power demand map of the engine, shown in Fig. 4a, very well within the range defined above. Recall that using this engine map corresponds to the assuming an existing automatic gearbox, which selects the most economic gear for a given rotational frequency. Note that this is justified as the eco routing problem described in Section 4 uses the fuel demand as objective function which is linearly correlated with the power demand of the engine.

3.4 Model Summary

This section summarizes the vehicle model presented in Sections 3.1, 3.2, and 3.3. Recall that the model has to be solved on every arch $a \in \mathcal{A}$ of the graph $\mathcal{G} = (\mathcal{N}, \mathcal{A})$ described in Section 2. Here, we summarize the vehicle model without indexing to indicate the arc a on which the model is solved.

The vehicle model is a differential-algebraic equation system of the form

$$\begin{aligned}
\left.\frac{\mathrm{d}\boldsymbol{z}}{\mathrm{d}t}\right|_t &= \boldsymbol{f}(\boldsymbol{z}(t), \boldsymbol{y}(t), \boldsymbol{u}(t), \boldsymbol{p}),\\
\mathbf{0} &= \boldsymbol{g}(\boldsymbol{z}(t), \boldsymbol{y}(t), \boldsymbol{u}(t), \boldsymbol{p}),
\end{aligned} \tag{14}$$

comprising four differential equations, i.e., $\boldsymbol{f}(\boldsymbol{z}(t), \boldsymbol{y}(t), \boldsymbol{u}(t), \boldsymbol{p}) \in \mathbb{R}^4$ and 11 algebraic equations, i.e., $\boldsymbol{g}(\boldsymbol{z}(t), \boldsymbol{y}(t), \boldsymbol{u}(t), \boldsymbol{p}) \in \mathbb{R}^{11}$. The four differential states $\boldsymbol{x}(t) \in \mathbb{R}^4$ are the distance s, speed v, SOC ξ, and fuel demand m_{fuel}. The model comprises 14 algebraic variables, 13 of the algebraic variables are real numbers and one is the binary variable β from the electric motor model (6), i.e., $\boldsymbol{y}(t) \in \mathbb{R}^{14} \times \{0, 1\}$. The variable β is defined by the constraints (6b) and (6c), which are omitted in (14), although they are part of the model. These constraints are embedded in the routing optimization problem, as will be shown in Section... Consequently, two variables can be defined as manipulated variables $\boldsymbol{u}(t) \in \mathbb{R}^2$. An intuitive and suitable choice would be, e.g., the acceleration a and either the torque of the electric motor T_{m} or the incoming torque of the gear box T_{gb}. In the routing optimization problem, these variables are used

to minimize the respective objective function, e.g., the fuel demand for driving the entire route in case of eco-routing.

With the original electric motor model (5), the DAE (14) would be nonsmooth, cf., e.g., [30]. Here, we use the formulation with the binary variable β, which introduced the constraints (6b) and (6c).

4 Integrated Routing and Power Management Optimization

This section presents the integrated eco routing and power management optimization approach, i.e., the formulation of the routing optimization problem in line with the assumption we make to solve the routing optimization problem.

The routing optimization problem is subject to routing constraints and to the vehicle powertrain model presented in Section 3. We formulate this integrated routing optimization problem as

$$\min_{\boldsymbol{x},\boldsymbol{z},\boldsymbol{y},\boldsymbol{u}} \ \varphi(\boldsymbol{z}(\boldsymbol{t}_f),\boldsymbol{x}), \tag{15a}$$

$$\text{s.t.} \sum_{a\in\mathcal{A}} (E_{n,a} - L_{n,a}) \cdot x_a = S_n, \ \forall\ n \in N, \tag{15b}$$

$$\sum_{a\in\mathcal{A}} (E_{n,a} + L_{n,a}) \cdot x_a \leqslant 2, \forall n \in \mathcal{N}, \tag{15c}$$

$$\left.\begin{aligned} \left.\frac{\mathrm{d}\boldsymbol{z}_a}{\mathrm{d}t_a}\right|_{t_a} &= \boldsymbol{f}(\boldsymbol{z}_a(t_a),\boldsymbol{y}_a(t_a),\boldsymbol{u}_a(t_a),\boldsymbol{p}) \\ \boldsymbol{0} &= \boldsymbol{g}(\boldsymbol{z}_a(t_a),\boldsymbol{y}_a(t_a),\boldsymbol{u}_a(t_a),\boldsymbol{p}) \end{aligned}\right\}, \forall t_a \in T_a, \forall a \in \mathcal{A}, \tag{15d}$$

$$\boldsymbol{0} = \boldsymbol{I}(\boldsymbol{z}_a(t_{a_1,0}),\boldsymbol{z}_a(t_{a_2,f}),\boldsymbol{x}), \forall a_1 \in \mathcal{A}, a_2 \in \mathcal{A}, \tag{15e}$$

$$\boldsymbol{0} \leqslant \boldsymbol{h}(\boldsymbol{z}_{a_1}(t_{a_1}),\boldsymbol{y}_{a_1}(t_{a_1}),\boldsymbol{z}_{a_2}(t_{a_2}),\boldsymbol{y}_{a_2}(t_{a_2}),\boldsymbol{x}), a_1 \in \mathcal{A}, a_2 \in \mathcal{A}, t_{a_1} \in T_{a_1}, t_{a_2} \in T_{a_2}, \tag{15f}$$

with the time horizon $T_a = [t_{a,0}, t_{a,f}]$. Recall that the constrains (15d) embed the vehicle model presented in Section 3, which has to be solved on every arc $a \in \mathcal{A}$ of the graph $\mathcal{G} = (\mathcal{N}, \mathcal{A})$ described in Section 2. The initial conditions for the vehicle model DAE are provided by the constraints (15e) on every arc a_1. The may depend on states of other arcs a_2, either in the manner of a continuity condition, i.e., to connect two adjacent arcs, or to define initial state values of the vehicle model DAE at the starting node of the graph $\mathcal{G}$. Notice that these constraints allow to model plugin hybrid electric vehicle, i.e., to model battery charging at the beginning of an arc. The constraints (15f) as path constraints or point constraints over and arc a_1 depending on state values of an arc a_2, e.g., an adjacent arc of arc a_1.
The objective function φ is flexible. For the eco route, we select the fuel demand for driving the route defined by the realization of $\boldsymbol{x}$ and we refer to the optimization problem (15) as the eco routing optimization problem. The battery SOC is only used in the constraints and the battery capacity can hence be fully exploited within desired ranges. For the shortest route, we select the length of the route and we refer to the optimization problem (15) as the shortest routing optimization problem. For the fastest route, we select the travel time of the route and we refer to the optimization problem (15) as the fastest routing optimization problem. We can easily change or extend the objective function, e.g., using the battery SOC or a weighted sum of fuel demand and battery SOC in the objective function. The objective function can also comprise state values at distinct nodes or a sum of state values of multiple nodes.
To compare the routes in terms of the fuel demand, we minimize the fuel demand of the fastest route and the shortest route for a fixed route. I.e., when we refer to the fastest route and shortest route, we refer to these routes with optimized fuel demand. For this, we calculate the shortest/fastest route first and then solve the routing optimization problem with a fixed route, to minimize the fuel demand. In addition, we solve the eco routing optimization problem with constraining the travel time by an upper bound as a benchmark.

(15) is a mixed-integer dynamic optimization problem (MIDO), cf. [31, 32]. Optimization problems of this problem class could be solved using algorithms for dynamic optimization, e.g., [33]. However, MIDOs are computationally challenging to solve, in particular, as the problems we are interested in here will easily grow to large-scale problems including large graphs. Therefore, we make the following assumptions to simplify (15).

Assumption 1 (Quasi-Stationarity) *We assume quasi-stationary transition, i.e.,*

$$\left.\frac{\mathrm{d}v}{\mathrm{d}t}\right|_t = 0.$$

Assumption 2 (Vehicle-Speed) *We assume the vehicle drives at the speed limit of the corresponding street.*

With Assumption 1, the longitudinal dynamic equation (2) becomes algebraic and defines the traction force F_t. Further, the travel distance equation (3) can be solved easily yielding a linear equation to define the travel time for arc a as $\Delta t_a = t_{a,f} - t_{a,0} = s_a/v_a$. The only remaining differential equation is the equation for the battery SOC (8). Due to Assumption 1, the battery power P_b is time-invariant and (8) can, in turn, be solved analytically, yielding an equation linear in the battery power P_b and in the SOCs $\xi(t_{a,0})$ and $\xi(t_{a,f})$. Alternatively, we could apply a discretization approach to the differential equations in the routing optimization problem (15), e.g., collocation, cf. [24], to (8), and solve the optimization problem (15) in the manner of a full discretization approach [34]. As a result, the vehicle model (15d) becomes an algebraic nonlinear equation system. Consequently, (15) becomes an MIQCP. Due to Assumption 2, we assign the velocity, thereby transforming the velocity from a manipulated variable to a parameter in the optimization problem (15). Therefore, we can calculated the forces in (2) a priory and assign them in the optimization problem, and thereby excluding the quadratical equation for the aerodynamic resistance force (1) from the optimization problem. The approach can easily be used without both assumptions 1 and 2. However, this complicates the routing optimization problem to be solved and hence imposes requirements on the optimization problem solution approach. Assumption 2 can easily be replaced by different velocity values, e.g., using a traffic model that is solved a priori to the routing optimization problem and gives different velocity values based on the current traffic state, cf., e.g., [7].

In summary, using the hybrid model in the routing optimization problem and applying the transformations above, we obtain a mixed-integer bilinear program (MIBP) where the bilinear terms are products of integer variables and continuous variables. We apply an exact linearization to the bilinear terms using a big-M reformulation, cf. [35], and obtain an equivalent mixed-integer linear program (MILP). We refer to this routing optimization problem as routing-MILP. The routing-MILP includes $14\ N_a + N_n + 3$ continuous variables, $2\ N_a$ binary variables, and $23\ N_a + 3\ N_n + 5$ constraints. In contrast, using the original mechanistic model instead of the hybrid model, which we developed based on the mechanistic model, and applying the same assumptions, we obtain an MIQCP. We refer to this routing optimization problem as routing-MIQCP. The routing-MIQCP includes $(2 + N_\gamma)N_a$ binary variables, $31\ N_a + N_n + 3$ continuous variables, and $43\ N_a + 3\ N_n + 5$ constraints.

5 Case Studies

We present three case studies applying the routing optimization approach presented in Section 4: one illustrative case study and two realistic case studies. The realistic case studies have been selected to prototypical travel scenarios: urban and rural/inter-urban. The following describes the case study framework and setup.

We acquire the data (nodes and arcs, node altitudes, longitudes, arc speed limits) using OpenStreetMap [19] to generate the directed graphs. The node elevations can be obtained from open-elevation [20]. We perform a preprocessing to calculated the required transition forces on the arcs and to cluster graph nodes within a certain distance range. We formulate the routing optimization problems in pyomo [28, 29] and solve the routing optimization problems using Gurobi [27] with the default optimality tolerances of 10^{-4}. We provide the framework for downloading the graph, preprocessing, and solving the routing optimization problem under `https://git.rwth-aachen.de/avt-svt/public/optimal-routing` including the three case studies presented in this section.

Table 1 presents the values of the model parameters for the case studies. They are based on vehicle parameter values in [21]. We assign the SOC at the starting node to be at 0.5 and use a constraint h, so

that the SOC at the end node is at least at 0.5. Other values could also be used to constrain the SOC during routing. The SOC is further constrained to be between zero and one on every arc and node.

In addition to the eco route, shortest route, and fastest route, we add to the routing-MILP an upper bound for the travel time and indicate the resulting route as eco route (tc) or shortest route (tc) depending on whether to objective function of the routing-MILP is the corresponds to the fuel demand or to the travel distance, respectively. Furthermore, we use as a benchmark the eco route where only the engine is used, i.e., no hybrid mode, neither transition nor recuperation, is used. For this, we remove those equation corresponding to the electric powertrain from the routing-MILP. We indicate the resulting route as eco route (engine only).

The first case study in Section 5.1 is an illustrative case study demonstrating the integrated routing and power management approach, and showing the validity of the hybrid model. The second case study in Section 5.2 is a routing case study in an urban region and shows that the integrated routing and power management approach can be applied to real world problems. The third case study in Section 5.3 demonstrates long distance routing characteristics including the effect of speed limits and the trade-off between travel time and fuel demand.

All solution times reported were obtained on a 64-bit Windows 10 desktop computer with an Intel Core i7-8700 CPU at 3.20 GHz and 16 GB RAM.

Table 1: Model parameter values for case studies.

parameter	**value**	**unit**
ρ_a	1.19	$\mathrm{kg/m^3}$
c_d	0.327	-
A_f	2.174	$\mathrm{m^2}$
m_v	1681	kg
g	9.81	$\mathrm{m/s^2}$
c_r	0.008	-
r_w	0.317	m
$\mathbf{\Gamma}_\mathrm{gb}$	$(12.38, 8.98, 6.45, 4.57, 3.32)$	-
η_c	0.95	-
η_m	0.9	-
γ	11	-
$P_{\mathrm{e},0}$	1000	W
κ_1	400	V
κ_2	40	V
κ_3	0.01	Ω
κ_4	-0.005	Ω
η_C	0.95	-
Q_0	$4.5 \cdot 3600$	As
H_fuel	$46{\cdot}10^6$	J/kg
ω_e^*	4186	1/s
$\kappa_{\mathrm{e},0}$	354.2857	W
$\kappa_{\mathrm{e},1}$	0.5785	Nm
$\kappa_{\mathrm{e},2}$	0.42	-
$\kappa_{\mathrm{e},3}$	$-3.9948 \cdot 10^{-9}$	$\mathrm{s^2}$
$P_\mathrm{e}^\mathrm{max}$	130	kW

5.1 Illustrative Case Study

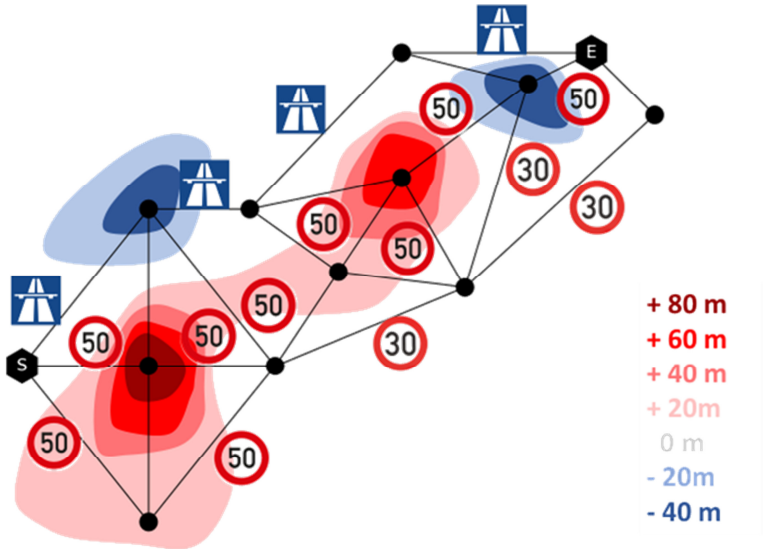

Fig. 5: Route map for illustrative case study. Colored background indicate node altitudes. White/transparent background indicates 0. Traffic signs indicate speed limits. The speed limit at highways (blue road signs) is set to 130 km/h.

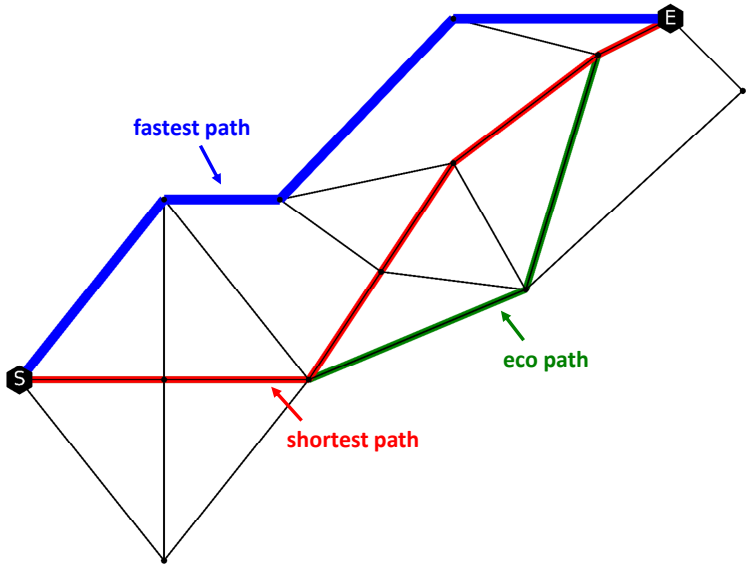

Fig. 6: Optimal routes for illustrative case study.

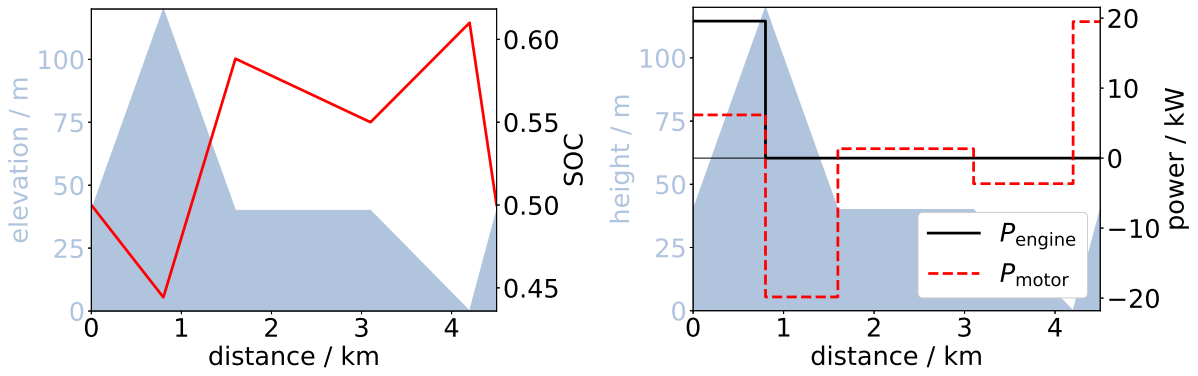

(a) (b)

Fig. 7: Optimal profiles of selected variables for illustrative case study.

Table 2: Results of route optimizations for illustrative case study. *Lower bound solution not converged to global optimality in CPU time limit of 42000s. Δ fuel demand is the relative difference of the optimal fuel demand with respect to the eco path fuel demand.

	CPU time / s	fuel demand / g	Δ fuel demand / %
shortest route	0.3	100	+ 12.56 %
fastest route	0.4	251	+ 182.63 %
eco route	0.39	88.81	0
eco route (mechanistic model)	42000*	88.12	- 0.78 %
eco route (engine only)	0.4	121.51	+36.82

This case study illustrates the integrated routing and power management approach and demonstrates the validity of the hybrid model. The map of the illustrative case study is shown in Fig. 5 including the arcs and nodes of the graph, and the contour lines indicating the node altitudes. The graph includes 13 nodes and 48 arcs. Therefore, the routing-MILP includes 96 binary variables, 688 continuous variables, and 1148 constraints. Therefore, the routing-MIQCP includes 336 binary variables, 1504 continuous variables, and 2108 constraints.

Fig. 6 shows the three paths resulting from the solution of the routing-MILP. All paths differ from each other. The fastest path uses the highways, whereas the eco path deviates slightly from the shortest path. Fig. 7 shows the SOC profile and the profiles of the engine and motor power usage. The results are reasonable: the battery is charged when the vehicle drives in downhill directions and used (discharged) otherwise, see Fig. 7a. As expected, the SOC is at 0.5 in the beginning and in the end. In the beginning, both engine and motor are used to provide the required traction force, see Fig. 7b. Afterwards, the vehicle is driven using the electric motor only. A negative power usage of the electric motor indicates that the battery is charged.

Table 2 provides the numerical results of the case study. Wee see that the shortest path requires about 1.8 times and the fastest path about 13 % more fuel than the eco path. Recall that both shortest and fastest route are optimized to minimize the fuel demand. The shortest path, fastest path, and eco path can be solved in less than 0.5 seconds. Table 2 shows in addition, that the eco route without hybrid powertrain operation (engine only) results in a fuel demand higher by more than 30 %, which demonstrates that large portions of the fuel demand savings are due to hybrid operation. In other words, the fuel demand can already be reduced drastically by applying a suitable powertrain management/operation strategy, i.e., without routing (shortest route admits lower fuel demand than eco route (engine only)). However, exploiting the full potential requires integrated optimal routing and powertrain management.

To validate the developed hybrid model, we compare the results of the routing-MILP with the results of the routing-MIQCP. Recall that the routing-MILP embeds the hybrid model whereas the routing-MIQCP embeds the (original) mechanistic model, which the hybrid model is built on. The results of

both problems are almost identical: They achieve the same paths and operation profiles and the optimal objective function values deviate only slightly. However, the routing-MIQCP requires significant more time to be solved. It did not converge within twelve hours to the desired optimality tolerances. There is, hence, a significant speed-up of more than 10^5 due to solving the routing optimization problem with hybrid model embedded. Thus, we can conclude the validity of the hybrid model and its superiority over the mechanistic model in terms of solution times, i.e., tractability in optimization.

The case study results show that we can apply the integrated optimal routing and power management approach based on the hybrid model yielding reasonable/intuitive results and large fuel demand reductions.

5.2 Urban Case Study

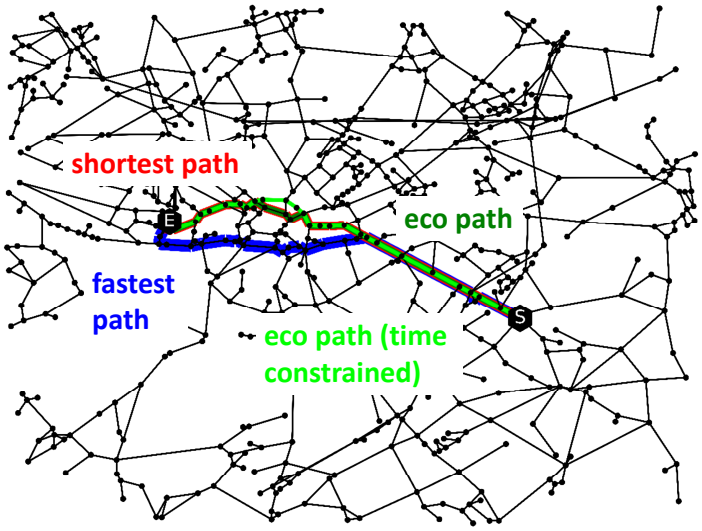

Fig. 8: Optimal routes for urban case study.

Table 3: Results of route optimizations for urban case study. *Lower bound solution not converged to global optimality in CPU time limit of 10800 s. **Final upper bound (feasible solution). (tc) indicates that the problem is solved with path time constraint.

	CPU time / s	fuel demand / g	path time / s	Δ fuel demand / %
shortest route	0.62	101.6	730	+ 2.2
fastest route	0.68	111.5	637	+ 12.2
eco route	10800*	99.4**	738	0
eco route (tc)	33	102.8	689	+ 3.4
shortest route (tc)	1.3	104.1	681	+ 4.7
eco route (engine only)	2.03	140.7	738	+ 41.54

This case study demonstrates the application of the integrated optimal routing and power management approach in a real urban environment, i.e., driving through Aachen/Germany. The graph comprises 659 nodes and 1802 arcs. Consequently, the routing-MILP includes 3604 binary variables, 25890 continuous variables, and 43428 constraints. In this case study, we add a constraint to the routing optimization problem to restrict the travel time to maximum 110 % of travel time required for the fastest route. Those problems with the time constraint are indicated by (tc). I.e., we solve the fastest route problem first and

obtain the travel time of the fastest route. We use this value to constrain the travel time in the shortest route and eco route optimization problems.

Fig. 8 shows that different routes results from the different routing problems. In particular, the fastest route strongly diverges from the other routes. The other routes are closer to each other.

Table 3 presents the numerical results of the case study. We see, again, that shortest route differs strongly from the other routes in terms of the fuel demand, and fastest route and eco route have similar fuel demand values. The results reveal further that the fuel demand savings of the eco route are at the expense of the travel time. It is, hence, motivated by practical reasons to restrict the travel time. Both shortest and fastest route require more than 110 % of the travel time of the fastest path. With travel time constrained to maximum 110 % of the travel time of the fastest path, the routes become closer, cf. Fig. 8 and Table 3. However, the time constrained shortest route and eco route require still drastically less fuel than the the shortest route. Table 3 shows further that adding the time constraint has an advantageous effect on the solution time. While the eco route could not be solved to the desired optimality tolerances withing 3 hours, the eco routing optimization problem with time constraint (tc) converged in about 30 s with time constraint. The shortest route and fastest route can be calculated in just about one second and are thus solved faster by approximately one order of magnitude compared to the eco route (tc). The fast solution time and comparable fuel demand justifies to use the shortest route (tc) in time critical applications instead of the eco route (tc). Moreover, Table 3 demonstrates the advantage of hybrid vehicles in urban environments. The eco route without hybrid powertrain (engine only) requires more than 40 % more fuel than the eco route and is even worth than the fastest route with respect to the fuel demand. I.e., in urban environments, the fuel demand can drastically be reduced by optimal management for the hybrid powertrain, while those parts of the fuel demand savings associated to the optimal routing are smaller compared to the savings associated by an optimal powertrain management.

Overall, the case study demonstrates that the integrated routing and power management approach can be applied to realistic cases with large graphs.

5.3 Long Distance Case Study

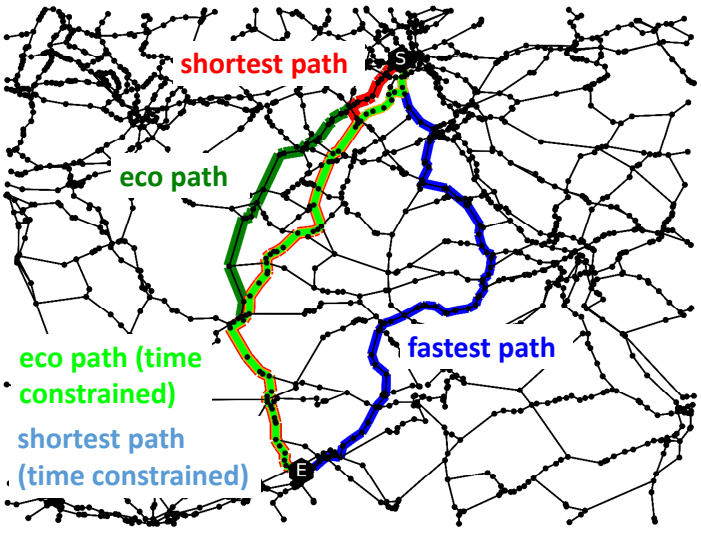

Fig. 9: Optimal routes for long distance case study.

In this case study, we demonstrate the application of the integrated routing and power management approach to and analyze the routing characteristics in a long distance case. Furthermore, we show the

Table 4: Results of route optimizations for long distance case study. *Lower bound solution not converged to global optimality in CPU time limit of 10800 s. **Final upper bound (feasible solution). (tc) indicates that the problem is solved with path time constraint.

	CPU time / s	fuel demand / kg	path time / s	Δ fuel demand / %
shortest route	0.4	4.24	6109	+ 19.59
fastest route	0.4	6.06	5236	+ 70.87
eco route	10800*	3.55**	8844	0
eco route (tc)	105	4.51	5736	+ 27.08
shortest route (tc)	0.6	4.51	5736	+ 27.08
eco route (engine only)	5.10	3.72	8844	+ 4.79

trade-off between travel time and fuel demand and the effect of highway speed limits. As long distance example, we aim at driving from Cologne to Trier/Germany. The map is illustrated in Fig. 9. The corresponding graph includes 1723 nodes and 4180 arcs. The routing-MILP, in turn, comprises 8360 binary variables, 60246 continuous variables, and 101314 constraints. As in the case study in Section 5.2, we constrain the travel time to be maximum 110 % of the the travel time of the fastest route, indicated by (tc).

Solving the routing-MILP yields the different routes depicted in Fig. 9. We see that the fastest route clearly diverges from the other routes, whereas the other routes are close to each other. Table 4 presents numerical results of the case study. It shows that the eco route drastically reduces the fuel demand compared to the other routes by at least about 20 %. The eco route and the shortest route require more than 110 % of the travel time of the fastest path. Furthermore, the eco route (without time constraint) cannot be solved to the desired optimality tolerance within three hours. Introducing the time constraint reduces the travel time and the cpu time required to solve the eco routing-MILP. As intended, the travel time of the shortest route and the eco route is reduced when the time constraint is used. Furthermore, introducing the time constraints, the eco routing problem (tc) is solved in just 105 seconds, i.e., results in a speed-up of solution time by approximately factor 100. Nevertheless, introducing the time constraints results in higher fuel demands. Apparently, the fuel saving is at the expense of travel time. This motivates analyzing the effect of time and speed limits in more detail, which is done in the following subsection. Moreover, Table 4 shows that the eco route without hybrid operation (engine only) results in a fuel demand only slightly higher than the fuel demand of the eco route with hybrid operation. I.e., for long distance routes, the contribution of the hybrid operation is only small and the eco route (engine only) can be used as a valuable approximation of the eco route.

5.3.1 Effect of Time and Speed Limits

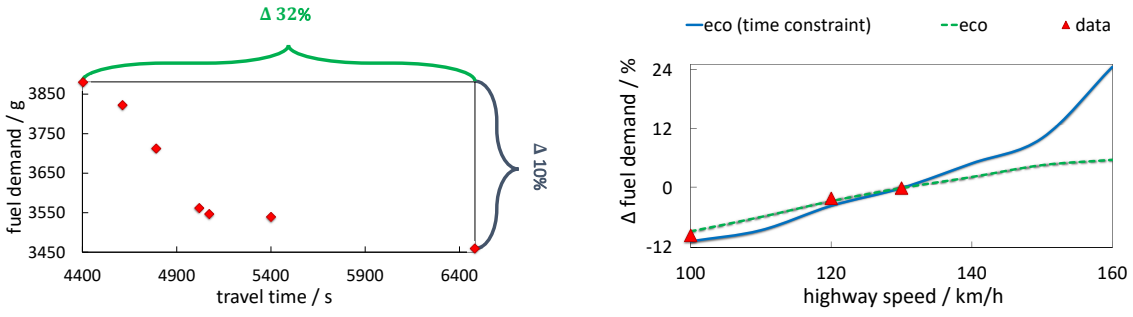

(a) (b)

Fig. 10: Effect of time based on long-distance case study. (a) Pareto frontier of fuel demand and travel time. (b) Fuel demand difference over highway speed limit. Data from [36].

We analyze the trade-off between travel time and fuel demand, and the effect of speed limits on highways on the basis on the previously presented case study in this subsection.

To analyze the trade-off between travel time and fuel demand, we formulate and solve a bi-objective optimization problem comprising of the constraints of the eco routing-MILP and the two objectives fuel demand and travel time:

$$\varphi = \begin{Bmatrix} \sum_{a\in\mathcal{A}} m_{\text{fuel},a}(t_{a,f}) \cdot x_a, \\ \sum_{a\in\mathcal{A}} t_{a,f} \cdot x_a \end{Bmatrix}. \tag{16}$$

We solve the resulting bi-objective routing optimization problem by applying an exact big-M linearization to (16), and solve the resulting problem with an ϵ-constrained method, cf. [37], to the eco routing problem with the same framework used in the other case studies, i.e., with pyomo [28, 29] and Gurobi [27]. For the ϵ-constrained method, we solve the eco route problem first and refer the ϵ-constraint to the travel time of the eco route. We then solve repeatedly the ϵ-constrained eco routing problem with decreasing values for ϵ, starting with one and terminating once the travel time is constrained to the value of the travel time of the fastest route resulting from the solution of the fastest routing-MILP.

The optimization results are illustrated in Fig. 10a, showing the pareto front, i.e., the trade-off between fuel demand and travel time: reducing the fuel demand comes at the cost of higher travel times. Increasing the fuel demand from its minimum value by 10 % results in time saving of about 30 %. This justifies the use of tight travel time constraints in the eco routing-MILP, which we have seen can drastically reduce the solution times of the eco routing-MILP. We see further that fuel demand savings up to approximately 8 % from the fuel demand of the fastest route fuel demand results in travel time losses of only about 10 %, whereas the remaining 2 % of fuel demand savings are much more expensive in terms of travel time. I.e., fuel demand savings can be obtained without disproportional time losses up to a certain point from which the travel time grow faster than the fuel demand reductions.

To analyze the effect of highway speed limits, we solve the eco routing-MILP of the long distance case study repeatedly with different speed limit values for the highways. The results of these optimizations are illustrated in Fig. 10b. The fuel demand savings are relative to the fuel demand resulting from the routing optimization problem with a speed limit of 130 km/h on the highways. We see that the speed limit on highways as the expected effect on the fuel demand. Also as expected, the fuel demand of the eco route is below the fuel demand of the eco route (tc), due to the trade-off between travel time and fuel demand as discussed above. We see that the fuel demand of the eco route (tc) increases superlinearly when the speed limit increases 150 km/h, whereas the fuel demand of the eco route becomes even sublinear. Latter is because the higher the speed limit on the highways is, the more attractive are routes apart from the highways in terms of fuel demand savings. As a consequence, solving the routing-MILP results in routes which uses less highways sections the higher the speed limit becomes, which in turn decreases the sensitivity of the highway speed limit on the fuel demand. Note, that this is induced by assigning the vehicle speed to the speed limit. Having the vehicle speed as a degree of freedom would likely reveal a different behavior, however, would also complicate the routing optimization problems. Fig. 10b additionally shows data from [36] for the fuel demand savings for different highway speed limits. Note, however, that the data relates to estimations of the effect of highways speed limits on the greenhouse gas emissions, whereas our predictions relate to the fuel demand (i.e., greenhouse gas emissions) of a single hybrid vehicle, which introduce a certain degree of blur in interpretation when compared to the data. Nevertheless, the data can be related to our predictions and matches the predictions of our integrated routing and power management approach well, which indicates the predictability and accuracy of the approach.

6 Conclusions

This article presents a direct integrated optimal routing and powertrain management approach that can be used, in particular, to calculate the ecologically optimal route for hybrid vehicles, i.e., the route leading to the minimum fuel demand by exploiting both the map and topology between starting point and destination as well as the power management of the hybrid vehicle. To predict the vehicle characteristics, we develop a hybrid model of the powertrain, which we embed in a routing optimization problem. The hybrid

model consists of mechanistic parts for those vehicle sections that can easily be modeled with mechanistic equations and data-driven parts for those vehicle sections which would lead to complex equation systems if modeled mechanistically. The hybrid model is developed based on a common mechanistic model of the vehicle powertrain. Using the hybrid model, based on a directed graph resulting from the map and topology, we formulate routing optimization problem, which, after reformulation, yields an MILP. Solving the MILP yields the ecologically optimal route, the fastest route, or the shortest route, depending on the objective function used.

We illustrate the application of the proposed routing approach in three case studies, including an illustrative small-scale case study, an urban case study, and a large-scale long distance case study.
The case studies demonstrate that the integrated routing and power management approach yields fuel savings of up to 70 % for realistic routing tasks and up to 50 % without sacrificing high travel time losses. In particular, drastic fuel demand savings are obtained in the long distance case study due to the large graph including many different route options including different street types with different speed limits. The eco routing optimization yields large savings for long-distant cases while in the urban case study the fuel demand savings are relatively small with fastest route requiring only 12 % more fuel than the eco route. The results allows to assess the effect of hybrid vehicles on the fuel demand for different route types. While hybrid operation leads to high fuel demand savings in urban environments, the effect of hybrid operation for long distances becomes very small. In other words, hybrid vehicles are ecologically advantageous compared to combustion based engines in urban regions whereas the advantage becomes smaller with increasing distance.
Furthermore, the results illustrate the trade-off between travel time and fuel demand: a lower fuel demand comes at the expense of a higher travel time. However, large fuel demand savings can already be realized with relatively small travel time losses.
The case study results further demonstrate the validity, i.e., high accuracy of the hybrid model with respect to the mechanistic model. The hybrid model leads to a speed-up in the solution time of the routing optimization problems of more than a factor of 10^5 as compared to the optimization with mechanistic model embedded, which is a MIQCP. The high accuracy and drastically improved computational tractability justify the use of the hybrid model. The results show further, that constraining the travel time of the route in the routing optimization problems by an upper bound further reduces the solution times of the routing optimization problem by a factor of approximately 100 compared to the time for the solution of the optimization problem without travel time constraint. This enables fast solution times for the solution of the routing optimization problem making the routing approach tractable in real and large-scale applications.
Although the hybrid model and the travel time constraints drastically reduce the time for the solution of the eco routing optimization problem, the real-time capable global solution cannot be guaranteed in all cases, especially, in case of very large-scale case studies. However, the results show, that the fuel demand optimized and time constrained shortest path yields an approximation of the time constrained eco route while can be solved very fast and achieve similar fuel demand savings. Furthermore, for long distance routes, the saving due to a hybrid vehicle operation become small and the eco route calculated without hybrid operation (engine only) yields, hence, a valuable approximation of the eco route with hybrid operation while the eco route (engine only) can be solved much faster allowing for real-time capability. An alternative would be, to take a local solution obtained after a predefined solution time limit.
The integrated optimal routing and powertrain management approach can be applied to evaluate the impact of different speed limits on highways. The corresponding results show that the highway speed limit has the intuitive effect on the fuel demand: reduced highways speed limits result in less fuel demands. The predicted fuel demand savings due to different speed limits agree well with expected values from literature, which further indicates the reliability of the developed hybrid model.
Overall, the results demonstrate that the proposed integrated optimal routing and powertrain management approach based on a hybrid model can reliably be applied to realistic routing tasks and reduces the fuel demand compared to the conventional fastest or shortest routes. The hybrid model allows for extrapolation and can easily be adapted to other powertrain architectures and characteristics of the battery and the engine.

Future work can apply the proposed approach in reality. This requires to adapt our approach to other HEV architectures. As fuel demand reductions directly translate into carbon footprint reductions, applying the eco routing strategy can help to further gain acceptance the hybrid vehicles due to increased sustainability. This requires to actually implement the routing optimization results (route and HEV operation) in reality during driving, directly or in form of setpoints to be tracked by a lower level HEV power management system. In addition, the application in reality requires recalculation of the optimal route when sufficiently large disturbances occur, e.g., traffic changes. The current traffic states can be calculated a priori to the routing optimization problem, using dynamic velocity models, cf., e.g., [7], yielding current velocity values on the respective roads. Our routing approach allows to assign target SOC values at specific nodes, e.g., at the end of the route, which allows to integrated the routing strategy in an overall framework using hybrid or electric vehicles as electricity buffers for grid stabilization, cf. [2]. Furthermore, future research can focus on improving the solution times for the problem class of the eco routing optimization problem to achieve real time capability for the solution of this optimization problem. In addition, future work can focus on accelerating the solution of the class of optimization problems with the mechanistic powertrain model, i.e., MIQCPs. This would enable to use the original mechanistic powertrain model in the routing approach directly. While we assumed quasi-stationary transition, future research can focus on the solution of the routing optimization problems without this assumption, i.e., with dynamic transition manipulating the HEV acceleration instead of its velocity.

Acknowledgments

This work was funded by the Deutsche Forschungsgemeinschaft (DFG, German Research Foundation) under Germany's Excellence Strategy, Exzellenzcluster 2186 "The Fuel Science Center". The authors thank Lukas Schmitt (Institute of Automatic Control at RWTH Aachen University) and Lukas Engbroks, Daniel Goerke, and Jan Philipp Schlomann (Daimler AG in Stuttgart/Germany) for fruitful discussions.

References

[1] C. C. Chan, "The state of the art of electric, hybrid, and fuel cell vehicles," *Proceedings of the IEEE*, vol. 95, no. 4, pp. 704–718, 2007.

[2] S. Nazari, F. Borrelli, and A. Stefanopoulou, "Electric vehicles for smart buildings: A survey on applications, energy management methods, and battery degradation," *Proceedings of the IEEE*, pp. 1–17, 2020.

[3] ADAC, "Elektroautos brauchen die Energiewende: Die Klimabilanz," *https://www.adac.de/verkehr/tanken-kraftstoff-antrieb/alternative-antriebe/klimabilanz/*, accessed 11/2020.

[4] C. Musardo, G. Rizzoni, Y. Guezennec, and B. Staccia, "A-ECMS: An adaptive algorithm for hybrid electric vehicle energy management," *European Journal of Control*, vol. 11, no. 4-5, pp. 509–524, 2005.

[5] S. Uebel, N. Murgovski, C. Tempelhahn, and B. Baker, "Optimal energy management and velocity control of hybrid electric vehicles," *IEEE Transactions on Vehicular Technology*, vol. 67, no. 1, pp. 327–337, 2018.

[6] L. Schmitt, M. Keller, T. Albin, and D. Abel, "Real-time nonlinear model predictive control for the energy management of hybrid electric vehicles in a hierarchical framework∗," in *2020 American Control Conference (ACC)*, IEEE, 2020.

[7] J. Guanetti, Y. Kim, and F. Borrelli, "Eco-routing of connected plug-in hybrid electric vehicles," in *2019 IEEE 58th Conference on Decision and Control (CDC)*, IEEE, dec 2019.

[8] M. M. Nejad, L. Mashayekhy, D. Grosu, and R. B. Chinnam, "Optimal routing for plug-in hybrid electric vehicles," *Transportation Science*, vol. 51, no. 4, pp. 1304–1325, 2017.

[9] M. Strehler, S. Merting, and C. Schwan, "Energy-efficient shortest routes for electric and hybrid vehicles," *Transportation Research Part B: Methodological*, vol. 103, pp. 111–135, 2017.

[10] A. Houshmand and C. G. Cassandras, "Eco-routing of plug-in hybrid electric vehicles in transportation networks," in *2018 21st International Conference on Intelligent Transportation Systems (ITSC)*, IEEE, 2018.

[11] A. Houshmand, C. G. Cassandras, N. Zhou, N. Hashemi, B. Li, and H. Peng, "Combined eco-routing and power-train control of plug-in hybrid electric vehicles in transportation networks," *https://arxiv.org/abs/2004.05161*, 2020.

[12] L. Zhen, Z. Xu, C. Ma, and L. Xiao, "Hybrid electric vehicle routing problem with mode selection," *International Journal of Production Research*, vol. 58, no. 2, pp. 562–576, 2019.

[13] C. Kurtulus and G. Inalhan, "Model based route guidance for hybrid and electric vehicles," in *2015 IEEE 18th International Conference on Intelligent Transportation Systems*, IEEE, 2015.

[14] M. Salazar, A. Houshmand, C. G. Cassandras, and M. Pavone, "Optimal routing and energy management strategies for plug-in hybrid electric vehicles," in *2019 IEEE Intelligent Transportation Systems Conference (ITSC)*, IEEE, 2019.

[15] G. D. Nunzio, A. Sciarretta, I. B. Gharbia, and L. L. Ojeda, "A constrained eco-routing strategy for hybrid electric vehicles based on semi-analytical energy management," in *2018 21st International Conference on Intelligent Transportation Systems (ITSC)*, IEEE, 2018.

[16] G. D. Nunzio, I. B. Gharbia, and A. Sciarretta, "A general constrained optimization framework for the eco-routing problem: Comparison and analysis of solution strategies for hybrid electric vehicles," *Transportation Research Part C: Emerging Technologies*, vol. 123, p. 102935, 2021.

[17] M. L. Thompson and M. A. Kramer, "Modeling chemical processes using prior knowledge and neural networks," *AIChE Journal*, vol. 40, no. 8, pp. 1328–1340, 1994.

[18] M. von Stosch, R. Oliveira, J. Peres, and S. Feyo de Azevedo, "Hybrid semi-parametric modeling in process systems engineering: Past, present and future," *Computers & Chemical Engineering*, vol. 60, pp. 86–101, 2014.

[19] OpenStreetMap Foundation, "Openstreetmap," *https://www.openstreetmap.org*, accesssed 04/2021.

[20] Open-Elevation, "A free and open-source elevation api.," *https://open-elevation.com/*, accessed 04/2021.

[21] L. Guzzella and A. Sciarretta, *Vehicle Propulsion Systems*. Springer Berlin Heidelberg, 2013.

[22] G. Rizzoni, L. Guzzella, and B. Baumann, "Unified modeling of hybrid electric vehicle drivetrains," *IEEE/ASME Transactions on Mechatronics*, vol. 4, no. 3, pp. 246–257, 1999.

[23] A. Caspari, L. Lüken, P. Schäfer, Y. Vaupel, A. Mhamdi, L. T. Biegler, and A. Mitsos, "Dynamic optimization with complementarity constraints: Smoothing for direct shooting," *Computers & Chemical Engineering*, vol. 139, p. 106891, 2020.

[24] L. T. Biegler, *Nonlinear Programming: Concepts, Algorithms, and Applications to Chemical Processes*. SIAM, 2010.

[25] Dassault Systemes, "https://www.3ds.com/de/produkte-und-services/catia/produkte/dymola/," accessed 04/2021.

[26] Mathworks, "MATLAB Polynomial curve fitting," https://de.mathworks.com/help/matlab/ref/polyfit.html, accessed 03/2021.

[27] Gurobi Optimization, "Gurobi 9.1," https://www.gurobi.com/, accessed 01/2021.

[28] W. E. Hart, J.-P. Watson, and D. L. Woodruff, "Pyomo: modeling and solving mathematical programs in python," *Mathematical Programming Computation*, vol. 3, no. 3, pp. 219–260, 2011.

[29] W. E. Hart, C. D. Laird, J.-P. Watson, D. L. Woodruff, G. A. Hackebeil, B. L. Nicholson, and J. D. Siirola, *Pyomo–optimization modeling in python*, vol. 67. Springer Science & Business Media, second ed., 2017.

[30] P. Stechlinski, M. Patrascu, and P. I. Barton, "Nonsmooth differential-algebraic equations in chemical engineering," *Computers & Chemical Engineering*, vol. 114, pp. 52–68, 2018.

[31] R. Allgor and P. Barton, "Mixed-integer dynamic optimization," *Computers & Chemical Engineering*, vol. 21, pp. S451–S456, 1997.

[32] J. Oldenburg, W. Marquardt, D. Heinz, and D. B. Leineweber, "Mixed-logic dynamic optimization applied to batch distillation process design," *AIChE Journal*, vol. 49, no. 11, pp. 2900–2917, 2003.

[33] A. Caspari, J. M. M. Faust, F. Jung, C. Kappatou, S. Sass, Y. Vaupel, R. Hannesmann-Tamás, A. Mhamdi, and A. Mitsos, "Dyos - a framework for optimization of large-scale differential algebraic equation systems," *Computer-Aided Chemical Engineering*, vol. 46, 2019.

[34] J. E. Cuthrell and L. T. Biegler, "On the optimization of differential-algebraic process systems," *AIChE Journal*, vol. 33, no. 8, pp. 1257–1270, 1987.

[35] L. T. Biegler, I. E. Grossmann, and A. W. Westerberg, *Systematic Methods of Chemical Process Design*. 1997.

[36] German Environment Agency, "Wirkung eines generellen Tempolimits auf Bundesautobahnen auf die Treibhausgasemissionen," https://www.umweltbundesamt.de/publikationen/klimaschutz-durch-tempolimit, vol. Texte | 38/2020, accessed 03/2021.

[37] K. Miettinen, *Nonlinear Multiobjective Optimization*. Boston, MA: Springer US, 1998.